Simulating turbulent transition using Large Eddy Simulation with application to underwater vehicle hydrodynamic modelling

Artur K. Lidtke*, **Stephen R. Turnock***, **Jon Downes***
FSI Group, University of Southampton, SO16 7QF, Southampton, UK
akl1g09@soton.ac.uk

1 Introduction

Large Eddy Simulation (LES) has been widely used by the aerospace community in order to model laminar separation bubbles (Uranga et al., 2011; Visbal et al., 2009) and other low Reynolds number phenomena.In maritime-related applications this family of turbulence modelling techniques has typically been used to model unsteady cavitation (Bensow, 2011).,Present work aims to apply it to develop first-hand experience with modelling laminar separation bubbles using LES in OpenFOAM, specifically looking at the effects of the choice of the subgrid model. The investigation is carried out on the SD7003 2D foil section, for which PIV flow field measurements, as well as reference CFD results, are available. Four different popular LES models are tested: Smagorinsky, dynamic k-equation, wall-adaptive (WALE), and implicit (ILES). The ultimate goal of this work is to apply the established methodology to model flows on underwater vehicle appendages, as well as propellers, which have been reported to experience noticeable amounts of laminar flow when operating at model-scale Reynolds numbers (Reverberi et al., 2016).These flows experience complex, unsteady hydrodynamic phenomena, such as tip and root vortices, laminar separation bubbles, and are affected by onset turbulence. Thus, studying them with LES could lead to improved predictions compared to the previous work by the authors which relied on using RANS transition models to simulate the flow past underwater vehicle geometries (Lemaire et al., 2016).

2 Methodology

2.1 Smagorinsky model

The turbulent viscosity subgrid model by Smagorinsky (1963) was first introduced in the context of weather modelling and has since seen wide adoption in many spheres of turbulence research. Its OpenFOAM implementation follows a different derivation than typically considered literature. It assumes local equilibrium and then uses the k-equation model formulaiton,

$$\mathbf{B} = \frac{2}{3}k\mathbf{I} - 2\nu_{SGS}\,dev(\overline{\mathbf{S}}). \tag{1}$$

Knowing that $\overline{\mathbf{S}} = \frac{1}{2}\left(\nabla\overline{\mathbf{U}} + (\nabla\overline{\mathbf{U}})^T\right)$, $\nu_{SGS} = C_k\sqrt{k}\Delta$, and $\overline{\mathbf{S}} : \mathbf{B} + \frac{C_e}{2\Delta}k^3 = 0$, the subgrid scale viscosity may be computed. The model thus makes use of two calibration constants, whose values were assumed in this work to be $C_k = 1.048$ and $C_e = 0.094$.

2.2 Wall-adaptive (WALE) model

The WALE model was derived by Nicoud and Ducros (1999) with the purpose of correctly modelling eddy viscosity near solid boundaries without the need for dynamic calculation of proportionality constants, making it attractive from accuracy and efficiency point of view. It has also been used to model transition, which is of particular interest in the present work. where V is the cell volume and $C_w = 0.325$ is a calibration constant. The model defines a modified filter length, $\Delta_S = C_w V^{\frac{1}{3}}$, The eddy viscosity is then computed as

$$\nu_{SGS} = \Delta_S^2\left(S_{ij}^d S_{ij}^d\right)^{\frac{3}{2}}\left[\left(\overline{S}_{ij}\overline{S}_{ij}\right)^{\frac{5}{2}} + \left(S_{ij}^d S_{ij}^d\right)^{\frac{5}{4}}\right]^{-1}. \tag{2}$$

In Eq. (2) $S_{ij}^d = \frac{1}{2}\left(\left(\frac{\partial u_i}{\partial x_j}\right)^2 + \left(\frac{\partial u_j}{\partial x_i}\right)^2\right) - \frac{1}{3}\delta_{ij}\left(\frac{\partial u_k}{\partial x_k}\right)^2$. The OpenFOAM implementation also requires constants C_k and C_e to be specified but these do not get used in the eddy viscosity computation.

2.3 Dynamic k-equation model

This model by Kim and Menon (1995) differs from the other two models considered so far in that it requires a transport equation for the subgrid turbulent kinetic energy to be solved,

$$\frac{\partial k}{\partial t} + \nabla \cdot (\mathbf{U}k) - \nabla \cdot (D_k \nabla k) = G - \frac{2}{3} k \nabla \cdot \mathbf{U} - \frac{C_e k^{\frac{3}{2}}}{\Delta} + S_k. \tag{3}$$

In Eq. (3) D_k is the diffusivity constant and C_e is not a constant but is instead dynamically computed based on the filter length and the rate of strain tensor. In the present work the inflow turbulence levels 0.2% were assumed to compute the inflow subgrid turbulence intensity.

2.4 Implicit model

The implicit LES (or ILES) approach does not attempt to formulate an expression for the effect of subgrid-scale eddies on the resolved flow. Instead, it relies on the dissipation provided by the mesh in order to emulate the added viscosity. It has been successfully used in cavitation (Bensow, 2011) and laminar separation (Visbal et al., 2009) modelling contexts and hence is of high relevance here.

3 Simulation set up

The simulation was carried out with chord length and inlet velocity having unit values, which allowed the Reynolds number to be adjusted by changing only the viscosity. This was assigned a value of $1.67 \cdot 10^{-5}$ m^2 s^{-1}, corresponding to a Reynolds number of 60,000, matching conditions in the experiments by Ol et al. (2005) and Burgmann et al. (2008). The angle of attack was set to 4° to match the experimental conditions. All simulations were initialised with a potential flow solution.

Structured meshes of C-grid topology were used, as shown in Figure 1. The grids extended 16 chord-lengths in away from the foil and span of 10% of chord was used, following simulations by Lemaire et al. (2016) who studied the same foil using RANS transition models and found little variation in predicted flow beyond this span-wise domain size. The first grid point away from the wall was located at y^+ of 0.2. The stream-wise and span-wise non-dimensional wall spacings were chosen as x^+=50 and z^+=15, respectively. This follows guidance from the literature which recommends (x^+,y^+,z^+)≤(130, 1, 30) (Choi and Moin, 2012). The resulting mesh constituted of 2.6 million cells, with 250 points placed along the chord and 20 in the span-wise direction. The LES filter length was computed based on the cubic root of the cell volume.

Second-order *fitleredLinear2V* convection and second-order *backward* time derivative schemes were used. Where necessary, additional transport equations were discretised using the first-order upwind scheme. Conservation of momentum and any additional quantities were solved using the preconditioned bi-conjugate gradient (*PBiCG*) solver, and the multigrid (*GAMG*) solver was used for pressure. Implicit pressure coupling algorightm PIMPLE was used to solve the unsteady flow with each of the equations being iteratively solved during several outer loops until L_1 norm residual of at most 10^{-7} has been reached. Time advancement was done by fixing the Courant number at 2.5 and letting the solver adjust the time step, which was typically around 0.001 s.

4 Results and discussion

Table 1 shows integral flow coefficients computed using the present simulations in comparison to reference experimental and numerical data. The predicted force coefficients may be seen to diverge by between 8 and 15% from the experimental data in terms of lift and between 30 and 50% for drag, with LES over-estimating both quantities. This trend is consistent for the LES data presented in the literature. Interestingly, the RANS simulations by Lemaire et al. (2016), while also over-predicting the forces, are closer to the measured values with a lift coefficient error of 5% and drag coefficient error of 35%. It may be seen that all the present models predict the location of separation to within 10% compared to each other and reference LES data. However, discrepancies with the experiments are much larger at up to 50% difference. One should note, however, that a very large spread of ±35% from the mean exists within the experimental measurements themselves, making exact quantitative comparison less certain. In terms of the position of reattachment, the range of error magnitudes compared to the experiments is greatly

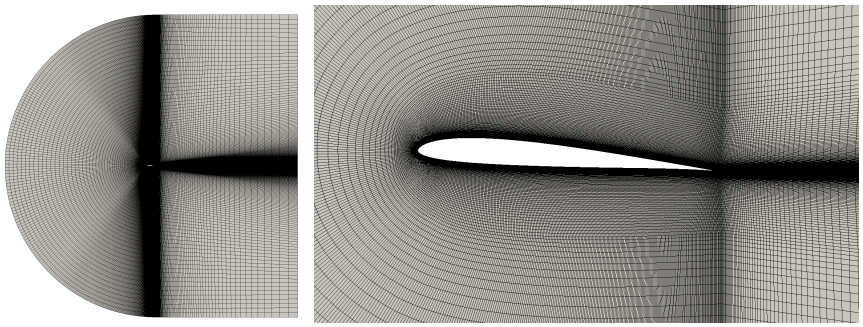

(a) C-type domain shape (b) Close up view of the foil mesh

Fig. 1: Overview of the numerical grid used for all computations.

reduced to between 18 and 32%, while for the reference LES data it varies between 12 and 15%. Notably, the discrepancy between the experiments themselves is also much smaller at approximately ±10%. This much better consistency between the present and published simulations and experiments indicates that the reattachment phenomenon is both better predicted and measured. No experimental data report mean force coefficients, but the present simulations agree well with the published LES data with the lift coefficient errors between 1% and 8%. For the unsteady RANS results by Lemaire et al. (2016) the discrepancy range grows to between 3% and 11%. For the drag coefficient the magnitude of differences between present and published LES data grows to between 9% and 30% and is approximately the same for the reference RANS data. In all cases, the WALE and dynamic *k*-equation models perform the best to the reference results.

Table 1: Comparison of integral flow coefficients for different tested LES models, as well as experimental and numerical data from the literature. Experimental data from Ol et al. (2005) and Burgmann et al. (2008), reference LES results from Visbal et al. (2009) and Uranga et al. (2011). RANS data with transition modelling from Lemaire et al. (2016).

Data set	$\overline{C_L}$	$\overline{C_D}$	x/c_{sep}	$x/c_{reattach}$	**RMS** C_L
Present simulations					
ILES	0.6609	0.0342	0.24	0.87	2.6744
Smagorinsky	0.6637	0.0344	0.24	0.88	2.1086
Dynamic k-equation	0.6078	0.0222	0.23	0.67	0.8819
WALE	0.6061	0.0220	0.23	0.65	0.8362
Public domain data					
Selig (Exp.)	0.5575	0.0154			
Burgmann (Exp.)			0.39	0.52	
IAR (Exp.)			0.33	0.63	
TU-BS (Exp.)			0.30	0.62	
AFRL (Exp.)			0.18	0.58	
Lemaire (LCTM URANS)	0.5851	0.0239	0.21	0.73	
Uranaga (ILES)	0.6122	0.0241	0.21	0.67	
Visbal (ILES)			0.23	0.65	
Xfoil	0.6250	0.0190	0.21	0.57	

The origin of these discrepancies may be better understood by analysing the mean distributions of axial velocity and turbulence intensity shown in Figure 2. The Smagorinsky and ILES models may be seen to significantly over-predict the extent of laminar separation, both in terms of the thickness and length of the bubble, compared to the experiments. The remaining two models predict velocity and turbulence iso-contours similar to those measured experimentally. A more quantitative assessment of this behaviour is presented in Figure 3, which depicts velocity cuts along several sections perpendicular

to the chord line of the foil. The data reveal close agreement between the WALE and dynamic k-equation models and the experiment, although the LES results appear to over-estimat the thickness of the laminar separation bubble by approximately 6% consistently over the entire length of the foil.

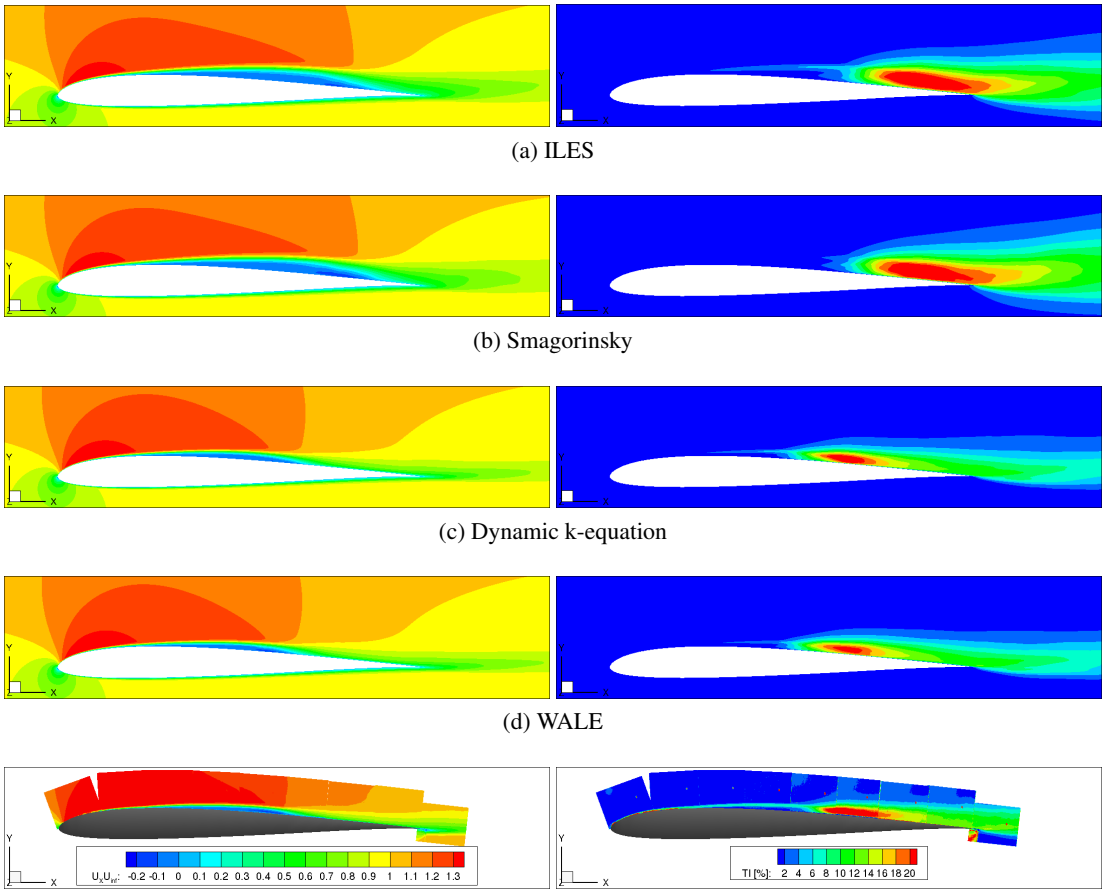

(a) ILES

(b) Smagorinsky

(c) Dynamic k-equation

(d) WALE

(e) Experiment

Fig. 2: Mean axial velocity (left) and turbulence intensity (right) contours at the mid-span of the foil for different LES models, including experimental PIV data by Burgmann et al. (2008). All sub-figures use the same colour scales as shown for the experiments. Turbulence intensity computed as $TI = \sqrt{\left|\frac{1}{3}\overline{u_i' u_i'}\right|}$.

It is interesting to note how the over-predicted size of the laminar separation bubble affects the unsteady nature of the flow. Figure 4 presents the time history and power spectral density functions of the predicted lift coefficient. The approximately 8% difference in mean C_L between the two simpler and two more complex considered models is easily discernible. One may also note how all models are affected by frequencies between Strouhal numbers of 0.18 and 0.22. However, the Smagorinsky and implicit methods predict a much more pronounced higher frequency content between St 1 and 4, and also predict prominent peaks at St of 0.55 which are not visible in the WALE and dynamic k-equation model data.

The origin of this behaviour is due to the models predicting larger separation bubbles also computing much larger coherent vortices in the wake of the foil. This may be seen in Figure 5 showing instantaneous iso-contours of the λ_2 criterion. Because the turbulence in the wakes predicted by WALE and dynamic k-equation models is much finer and approaches an isotropic state much faster, the unsteady load variations caused by them have less of an influence on the force coeffcient. This makes the principle shedding frequency at St of approximately 0.2 stand out much more in the energy spectra compared to the ILES and Smagorinsky models.

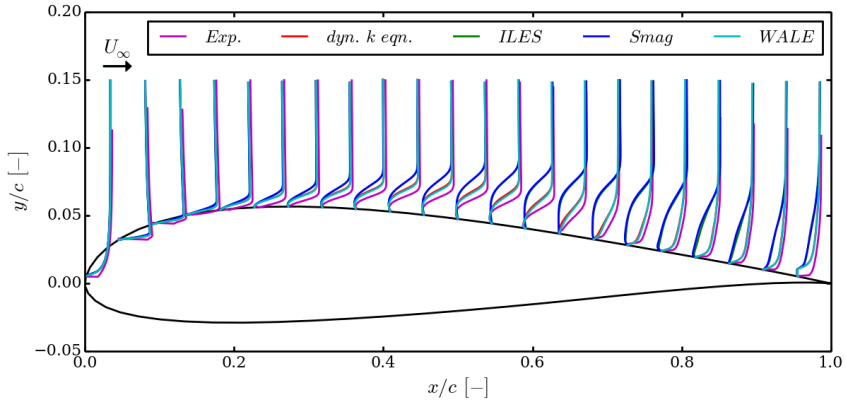

Fig. 3: Mean axial velocity at cuts spaced along the chord line of the foil.

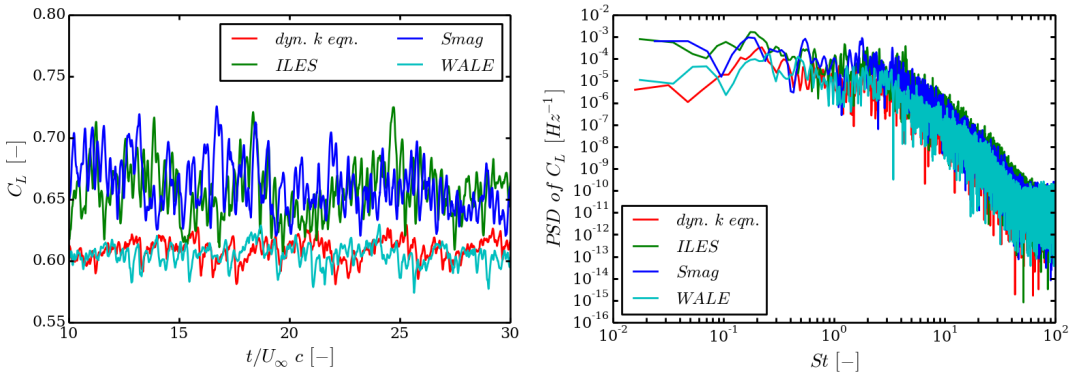

(a) Time history

(b) Power spectral density function

Fig. 4: Overview of the numerical grid used for all computations.

5 Conclusions

Comparison of the four different subgrid LES models has shown that the wall-adaptive eddy viscosity (WALE) and dynamic *k*-equation subgrid models perform better than their Smagorinsky and ILES counterparts at modelling flows undergoing laminar separation. This is evident from the size and position of the separation bubble being better with the former two models. For all models the vortices shed off from the trailing edge of the separation bubble are predicted to stretch the entire span-wise extent of the numerical domain. Due to the much larger size of the recirculating flow region in the case of Smagorinsky and ILES models, the predicted shed vortices are much larger and remain coherent further downstream.

The results have shown poor agreement with the experiments regarding the position of separation which is predicted to occur earlier than in the experiments with errors up to 50%. All of the models methods appear to be in good agreement with each other in this respect. Presence of significant discrepancies among the experimental measurements indicates difficulties in conducting quantitative measurements of this quantity, which somehwat discredits the argument against the accuracy of the numerical methods. Position of the reattachment is predicted better with errors around 20%, although it is found to occur further downstream than what was reported experimentally. The thickness of the recirculating flow region forming the laminar separation bubble is over-predicted by approximately 6% with respect to the measurements. The overall larger size of predicted laminar separaiton bubbles leads to over-estimation of the lift and drag coefficients, leading to errors of approximately 8% for the lift and 30% for the drag.

The computational expense to simulate 100 non-dimensional time units was approximately 120 CPU-hours per 10,000 cells and did not vary significantly between the different turbulence models. This, while

significant, indicates that with sufficient computational resources and mesh resolution the models should be capable of capturing transition and complex three-dimensional flow features on underwater vehicle appendages and model-scale propellers.

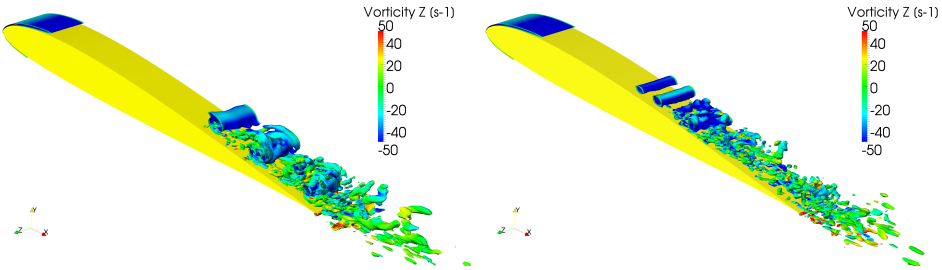

(a) ILES (b) WALE

Fig. 5: Comparison of instantaneous $\lambda_2 = -150$ iso-contours for two considered LES models showing the different predicted size of vortices shed off the trailing edge of the separation bubble. Coloured by the span-wise vorticity component indicating the amount of turbulent mixing.

Acknowledgements

The presented work has been funded as a part of the BRIDGES Project (http://www.bridges-h2020.eu/). This Project has received funding from the European Union Horizon 2020 research and innovation programme under grant agreement No 635359. The authors acknowledge the use of the IRIDIS High Performance Computing Facility, and associated support services at the University of Southampton, in the completion of this work and the use of OpenFOAM (http://openfoam.org/) for all of the simulations.

References

Bensow, R. (2011). Simulation of the unsteady cavitation on the the Delft Twist11 foil using RANS, DES and LES. In *2nd International Symposium on Marine Propulsors*, Hamburg, Germany, June.

Burgmann, S., Dannemann, J., and Schroder, W. (2008). Time-resolved and volumetric PIV measurements of a transitional separation bubble on an SD7003 airfoil. *Experiments in Fluids*, 44(4):609–622.

Choi, H. and Moin, P. (2012). Grid-point requirements for large eddy simulation : Chapman's estimates revisited. *Physics of Fluids*, 24.

Kim, W.-W. and Menon, S. (1995). A new dynamic one-equation subgrid-scale model for large eddy simulations. In *33rd Aerospace Sciences Meeting and Exhibit*, Reno, NV, USA.

Lemaire, S., Lidtke, A. K., Vaz, G., and Turnock, S. R. (2016). Modelling Natural Transition on Hydrofoils for Application in Underwater Gliders. In *19th Numerical Towing Tank Symposium (NuTTS)*, 3-4 October, St Pierre d'Oleron, France.

Nicoud, F. and Ducros, F. (1999). Subgrid-scale stress modelling based on the square of the velocity gradient tensor Subgrid-scale stress modelling based on the square of the velocity gradient tensor. *Turbulence and Combustion*, 62(3):183–200.

Ol, M. V., McCauliffe, B. R., Hanff, E. S., Scholz, U., and Kähler, C. (2005). Comparison of Laminar Separation Bubble Measurements on a Low Reynolds Number Airfoil in Three Facilities. *35th AIAA Fluid Dynamics Conference and Exhibit*, pages 1–11.

Reverberi, A., Lloyd, T., and Vaz, G. (2016). Towards cavitation modelling accounting for transition effects. In *219th Numerical Towing Tank Symposium (NuTTS)*, St Pierre d'Oleron, France.

Smagorinsky, J. (1963). General circulation experiments with the primitive equations I: the basic experiment. *Monthly Weather Review*, 91(3):99–164.

Uranga, A., Persson, P., Drela, M., and Peraire, J. (2011). Implicit Large Eddy Simulation of transition to turbulence at low Reynolds numbers using a Discontinuous Galerkin method. *International journal for numerical methods in engineering*, 87(October 2010):232–261.

Visbal, M. R., Gordnier, R. E., and Galbraith, M. C. (2009). High-fidelity simulations of moving and flexible airfoils at low Reynolds numbers. *Experiments in Fluids*, 46:903–922.